ARL-TR-9581 ● SEP 2022

DEVCOM ARMY RESEARCH LABORATORY

Design and Operation of a Solar Electrolysis System

by Matthew Weiner, Lucia Garcia, Bismi Khan,
Vijay Parameshwaran, David R Baker, and Jiangtian Li

NOTICES

Disclaimers

The findings in this report are not to be construed as an official Department of the Army position unless so designated by other authorized documents.

Citation of manufacturer's or trade names does not constitute an official endorsement or approval of the use thereof.

Destroy this report when it is no longer needed. Do not return it to the originator.

ARL-TR-9581 ● SEP 2022

Design and Operation of a Solar Electrolysis System

Matthew Weiner and Bismi Khan
University of Maryland, College Park

Lucia Garcia
University of Maryland, Baltimore County

Vijay Parameshwaran and David R Baker
DEVCOM Army Research Laboratory

Jiangtian Li
Oak Ridge Associated Universities

REPORT DOCUMENTATION PAGE

Form Approved
OMB No. 0704-0188

1. REPORT DATE *(DD-MM-YYYY)*	2. REPORT TYPE	3. DATES COVERED (From - To)
September 2022	Technical Report	30 May–5 August 2022

4. TITLE AND SUBTITLE
Design and Operation of a Solar Electrolysis System

5a. CONTRACT NUMBER

5b. GRANT NUMBER

5c. PROGRAM ELEMENT NUMBER

6. AUTHOR(S)
Matthew Weiner, Lucia Garcia, Bismi Khan, Vijay Parameshwaran, David R Baker, and Jiangtian Li

5d. PROJECT NUMBER

5e. TASK NUMBER

5f. WORK UNIT NUMBER

7. PERFORMING ORGANIZATION NAME(S) AND ADDRESS(ES)
DEVCOM Army Research Laboratory
ATTN: FCDD-RLS-CC
Adelphi, MD 20783-1138

8. PERFORMING ORGANIZATION REPORT NUMBER
ARL-TR-9581

9. SPONSORING/MONITORING AGENCY NAME(S) AND ADDRESS(ES)

10. SPONSOR/MONITOR'S ACRONYM(S)

11. SPONSOR/MONITOR'S REPORT NUMBER(S)

12. DISTRIBUTION/AVAILABILITY STATEMENT
Approved for public release: distribution unlimited.

13. SUPPLEMENTARY NOTES

14. ABSTRACT
A system connecting a commercial photovoltaic panel to a water electrolysis cell is designed as a demonstrator project for converting solar energy into hydrogen as a fuel. The electrical design is specifically tuned to drive a specified voltage to the electrolysis cell through control of buck converters and monitored through directly mounted voltmeters and ammeters. The electrolysis cell is designed in a H-cell configuration to contain the electrolyte. Gas collection bags are mounted on the electrodes to collect hydrogen gas evolved from water electrolysis. The components are constructed and mounted such that outdoor operation could be conducted without environmental damage to critical components. The synthesized electrocatalysts (undoped and iron-doped cobalt phosphide on nickel foam) are characterized with linear sweep voltammetry, cyclic voltammetry, and impedance spectroscopy to evaluate their performance. The electrodes are subsequently mounted within the electrolysis cell with potassium hydroxide electrolyte, and the entire photovoltaic panel/electronics/electrolysis cell system is tested outdoors to evaluate performance under a variety of environmental conditions. System performance is evaluated through calculations of Faradaic efficiency and energy conversion efficiency through the collection of hydrogen gas.

15. SUBJECT TERMS
Energy Sciences, solar energy, hydrogen, photovoltaics, electrocatalysis, fuels

16. SECURITY CLASSIFICATION OF:			17. LIMITATION OF ABSTRACT	18. NUMBER OF PAGES	19a. NAME OF RESPONSIBLE PERSON
a. REPORT	b. ABSTRACT	c. THIS PAGE			Vijay Parameshwaran
Unclassified	Unclassified	Unclassified	UU	36	19b. TELEPHONE NUMBER (Include area code) (301) 394-0927

Contents

List of Figures

List of Tables

1. Introduction

1.1 Background and Motivation

Energy is a critical component of Army operations in a variety of ways: generation, storage, distribution, and use. Power generation has historically relied on combustion of hydrocarbon fuels (such as JP-8): within military vehicles for movement and in electrical generators whose output is delivered to local grid networks. Fuel supply convoys, however, are susceptible to attacks by adversaries, adding a logistical burden. The ability to generate fuels onsite can reduce or remove the risk associated with supply logistics and will allow Army operations to be conducted untethered from externally delivered fuels and generators.

From the variety of locally available sources of energy within the scope of Army operations, solar has been shown to be ubiquitous and widely available, and is untethered from the convoy logistics that have compromised fuel delivery. Solar energy fits within the Multi-Domain Operations (MDO) framework of the Army,[1] in which several installations work off of microgrids that are powered off of a local energy source. The recently published Army Climate Strategy report[2] has emphasized the need to move toward carbon-free sources of energy, including solar.

The traditional implementation of solar energy has been with large-area panel arrays connected to an extensive electric grid network, but this model of energy generation and usage is not applicable in the Army. If, however, solar energy can supply microgrid sites or be used to charge battery packs for usage in electrified equipment and vehicles, then it would help achieve a vision for Army usage in the MDO. Implementations of solar with this vision could come in the form of panel arrays,[2] flexible "solar blankets" that are easily portable by mobile units,[3] or integrated micro- and nanoscale light absorber materials directly integrated into soldier gear and equipment.[4]

Solar energy can additionally be directly coupled to chemical reactions for fuels production, in which the fuels generated onsite can be used for a variety of applications. These fuels include hydrogen, which can be directly converted to electrical energy through fuel cells; syngas, a combination of hydrogen and carbon monoxide that is a feedstock to create higher-order hydrocarbon chemicals; alcohols such as ethanol and propanol; and ethyelene as a feedstock for polyethylene plastics production. Fuels, like battery packs, offer a solution of chemical energy storage that enables solar energy to be used in times and locations where it is not readily available. Unlike the fuels brought in through supply convoys

from offsite locations, many of the fuels created onsite through solar energy are created by electrochemical reduction of already-present carbon dioxide, thus helping to close the carbon cycle loop and minimize emissions. This ultimately helps to execute the Army Climate Strategy in achieving carbon-pollution free energy sources at the point of need.

Within the US Army Combat Capabilities Development Command Army Research Laboratory (ARL), a variety of research topics are currently being investigated for solar-to-fuels applicability. These include electrocatalyst synthesis for carbon dioxide reduction, plasmonic metal decoration for light-to-thermal/chemical energy transfer, and both electron microscopy and time-resolved optical spectroscopy to elucidate the properties of the materials and processes involved. As the Technology Readiness Level is scaled up, the eventual result of these research directions will be within a system demonstrator project. Therefore, designing a system that demonstrates the conversion of solar energy to chemical energy outside of a controlled laboratory environment is an important step of operationalizing science outside.

1.2 Demonstrator of Solar Electrolysis

The system chosen as a demonstrator basis for solar-to-fuels research at ARL is a commercial flexible photovoltaic (PV) panel coupled to a large-scale water electrolyzer. When placed outside, the solar energy absorbed in the panel will generate a voltage and current; the output voltage will undergo a step-down DC-DC conversion and drive a water electrolysis reaction within the electrolyzer:

$$2H_2O_{(l)} \rightarrow 2H_{2\,(g)} + O_{2\,(g)}$$

The generated chemical products are hydrogen and oxygen gas. Hydrogen is the important component of the fuel generated, as it can be stored and used later within fuel cells (oxygen can be supplied from the ambient air). Two electrodes, driving the anodic oxygen evolution reaction and the cathodic hydrogen evolution reaction, respectively, are coated with electrocatalysts to minimize the overpotential losses in driving the water electrolysis reaction with a DC voltage. Under full operation, the PV panel will source approximately 2 V (which takes into account the 1.23-V thermodynamic potential for water electrolysis plus some additional bias to account for overpotential losses) to the electrolyzer, and based on the electrocatalyst kinetics, hydrogen and oxygen gas will be generated at a rate that is matched by the current drawn by the electrolyzer from the PV panel.

By performing some calculations, it is possible to get an estimation of the gas generation and energy generation rates from this system. The hydrogen evolution half-reaction is taken in a base solution:

$$2H_2O_{(l)} + 2e^- \rightarrow H_{2\,(g)} + 2OH^-$$

To create one molecule of hydrogen, two electrons are required as an input. The input electrons to the reaction per unit time is analogous to an electric current being driven; electric current is charge per unit time, and each electron carries a charge of 1.6×10^{-19} C. Therefore, if the electrolyzer has a current I in units of A (C/s), it would be driving an electron flux of $I/1.6 \times 10^{-19}$ electrons/s. Since two electrons make one molecule of hydrogen, the hydrogen production rate would be $I/(2 * 1.6 \times 10^{-19})$ molecules per second. Invoking Avogadro's number to get the molar production rate, this would be $I/(2 * 1.6 \times 10^{-19} * 6.022 \times 10^{23})$ moles per second. Since hydrogen has a molar mass of 2 g/mol, the mass production rate of hydrogen would be $I/(1.6 \times 10^{-19} * 6.022 \times 10^{23})$ grams per second. With modifications to time and mass, this would be $(I * 3600)/(1000 * 1.6 \times 10^{-19} * 6.022 \times 10^{23})$ kilograms per hour. Therefore, various aspects of this system demonstrator can be tailored to produce a specific desired mass production rate of fuel.

Although it looks to be a straightforward process to connect the components of the system together to have a demonstrator for solar electrolysis, there are several engineering and design considerations to take into account. The subsequent sections in this report describe these considerations in more detail.

2. Components and Assembly

2.1 Overall System Design

There are four main design categories within this system: solar cell, electronics, electrolysis cell, and physical construction. Within this system, energy is generated from the solar cell, and moves through the electronics and into the electrolysis cell, which produces the end product hydrogen and byproduct oxygen gas. The job of the PV cell is to convert incident solar energy into electrical energy. The circuitry takes this electrical energy and regulates it to the desired voltage and current. The electrolysis cell then converts this electrical energy into chemical energy, which can be easily stored and used for fuel cells. Figure 1 shows the overall system design. The Appendix provides links to the parts that were purchased.

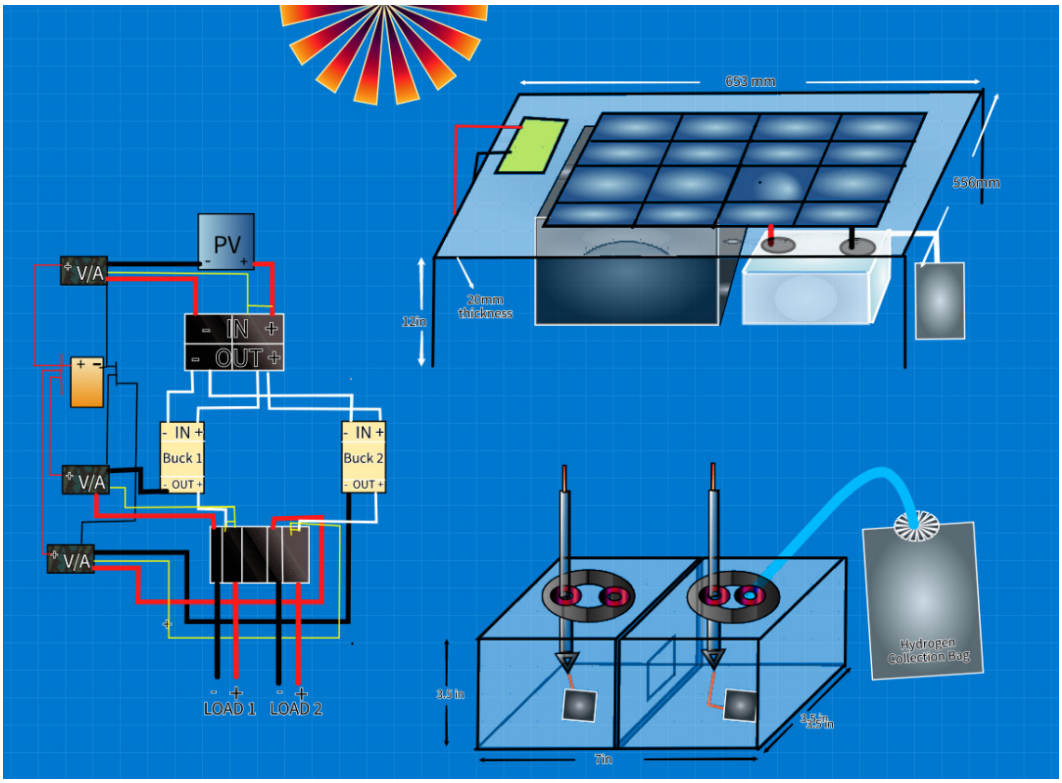

Fig. 1 Overall system design

2.2 Solar Cell

The first component is the solar cell. This system uses a SunPower SPR-E-Flex-50.[5] At standard test conditions of 25 °C, 1000 W/m^2, and air mass 1.5 solar radiation, the cell is rated for 50 W with a tolerance of ±3%, 17.7 V, and 2.8 A, with an open circuit voltage and short circuit current of 21.5 V and 3.1 A, respectively.

To connect the solar cell to the circuit electronics, MC4 connectors were used, because they are weather-resistant and can withstand a 20-A current, which is much greater than expected 2.8-A output from the solar cell. The male and female connectors were crimped on wires to securely connect the MC4 connectors.[6] On the other side of the wire, ring terminals are crimped on to connect them to a screw terminal block.

2.3 Electronics

The second component of the system is the electronics. For safety purposes, the electronics are mounted onto nonconductive wood blocks. The wood blocks do not pose a fire threat, because the temperature of the electronics will not exceed 60 °C. The goal of the electronics is to take the 17.7 V and 2.8 A and convert it to a voltage

and current for a desired output. For the demonstration of this electrolysis reaction, 2 V and about 1–2 A are used. To accomplish this, a ACEIRMC 20-A, 300-W CC CV step down module adjustable DC 6-40V to 1.2–36-V voltage regulator buck converters constant current power supply module is used (Fig. 2).

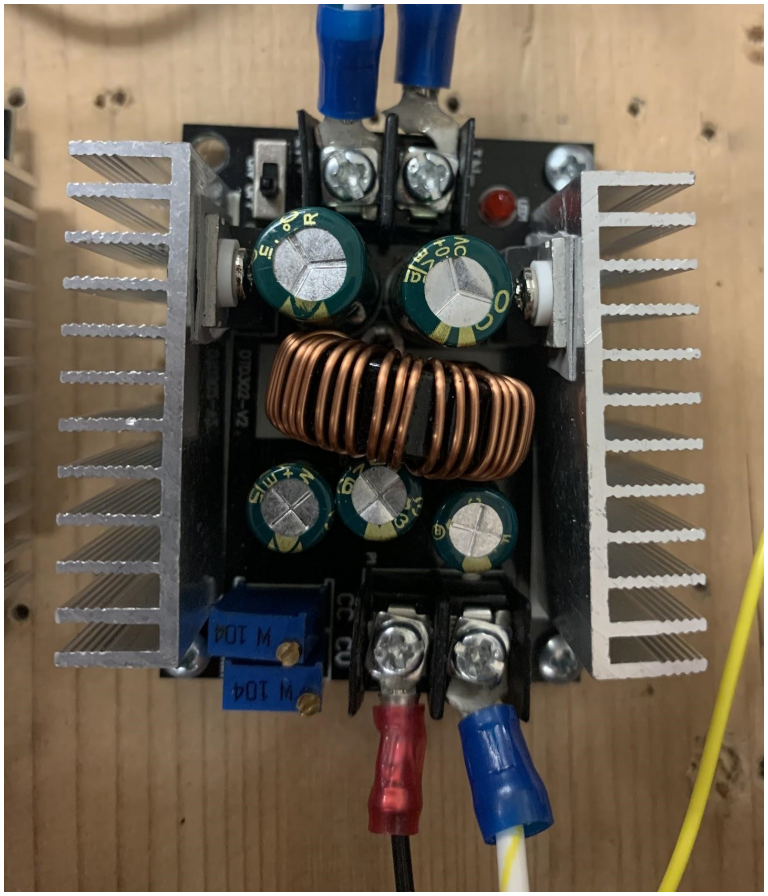

Fig. 2 Buck converter in circuit

Buck converters consist of a switch, diodes, inductors, and capacitors to control voltage and current across a load. The switch is controlled through pulse width modulation (PWM), where the percent of time closed is proportional to the percent of the voltage source supplied to the load. By varying the amount of time the switch is closed, this controls how much energy is received by the inductor. By controlling the PWM, inductance and capacitance of the converter, the desired output voltage and current can be tuned.[7]

These specific converters were chosen because they are rated for 300 W (which is much greater than what is being used) and have attached heat sinks. These two specifications reducing the risk for overheating. Also, these devices can apply constant voltage and current outputs. This means that as long as the solar cell is supplying more than 2 V, exactly 2 V can be output from one buck into the

electrolysis cell. The converters have roughly a 2.25- by 2.25-inch footprint, which is small enough to fit into our design constrained by the size of their box. For this demonstration, two buck converters are used, in which their inputs are connected in parallel from the solar cell output; their outputs, however, are connected to their own separate loads. This is important, because if two buck converters have connected outputs, current will only flow through one, short circuiting the others. As shown in Fig. 3, the positive and negative outputs of the solar cell are connected via screws to the terminal block and connected in parallel using red and black pre-insulated terminal barrier strips, respectively. The positive ends connect to the "In^{+}" connection on the buck converter and the negative ends connect to the "In^{-}" connection. The wire used to connect the two components is an 18-American wire gage (AWG) wire with #12 fork terminals crimped to each end. These wires can carry roughly 16 A, which is meets the tolerance of what is expected for them to carry at any point of operation.

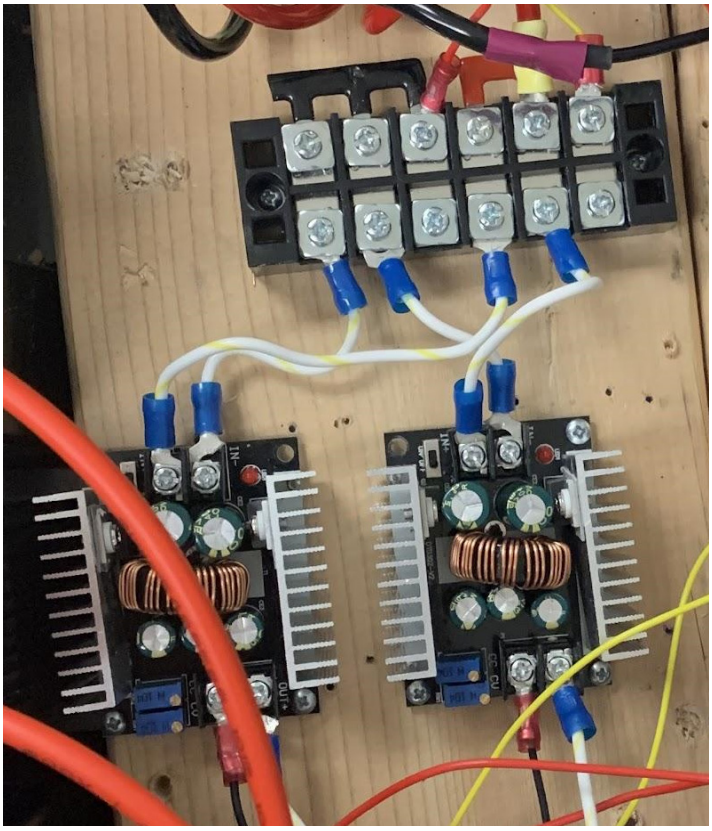

Fig. 3 Buck converters wiring

The outputs of the buck converter, as previously discussed, are attached to their own respective load. The outputs are attached to a similar screw terminal, also using 18-AWG wires with fork terminals. Out of the block terminal, 12-AWG wires are used to connect to the electrolysis cell (Fig. 4). Again, MC4 connectors are used,

because they are resilient in outdoor conditions and are protected from rain and other environmental effects.

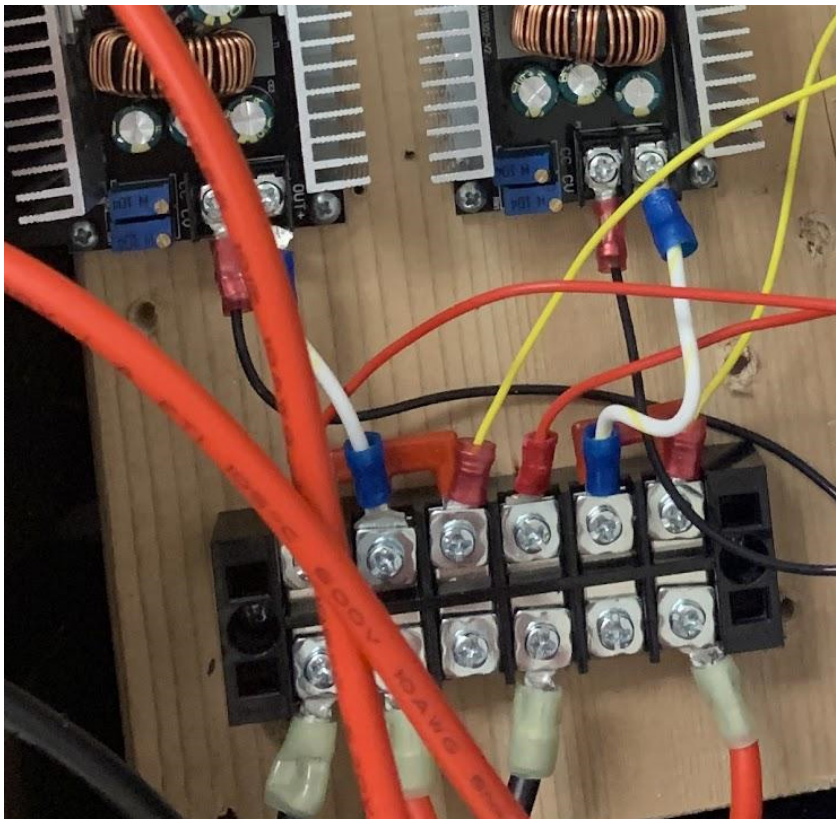

Fig. 4 Terminal connection downstream of buck converters

Currently, only between 2 and 4 of the 50 produced watts of power enter the electrolytic cell. This leaves room for the output of a buck converter to connect to an additional component such as a rechargeable battery, which can power the system when the solar cell is not receiving light. This battery would output energy back into the buck converters so that it can be regulated to the desired 2 V. This would allow for hydrogen to be produced at any time of the day and on days where the sun is not visible.

To measure the voltage and current coming out of the solar panel and each buck converter, three mini digital voltmeter ammeter DC 100-V, 10-A panels[8] were used. For each wire coming out of the volt/ammeter, 18-AWG wires were soldered to the ends in order to increase the available length of the wire. Also, heat shrink tubing was used to cover the exposed soldered wire to ensure safety of the circuit.

To connect the volt/ammeter to the circuit, there are five wires: red, black, yellow, thick red, and thick black. Current is measured through the return path of the circuit using the thick red and black wires. For example, to measure the current out of the

solar cell the negative output from the solar cell is connected to the thick black wire. The thick red wire is connected to the negative part of the screw terminal, which feeds into the negative of the buck converters. This means that the ammeter is connected in series with the solar cell within the cell's current return path.

To measure the voltage, the yellow wire is connected to the point where the voltage is to be read.

In Fig. 5, the top volt/ammeter reads the voltage and current from the solar cell, the bottom one reads the output of the left buck converter, and the middle reads the output of the right buck converter.

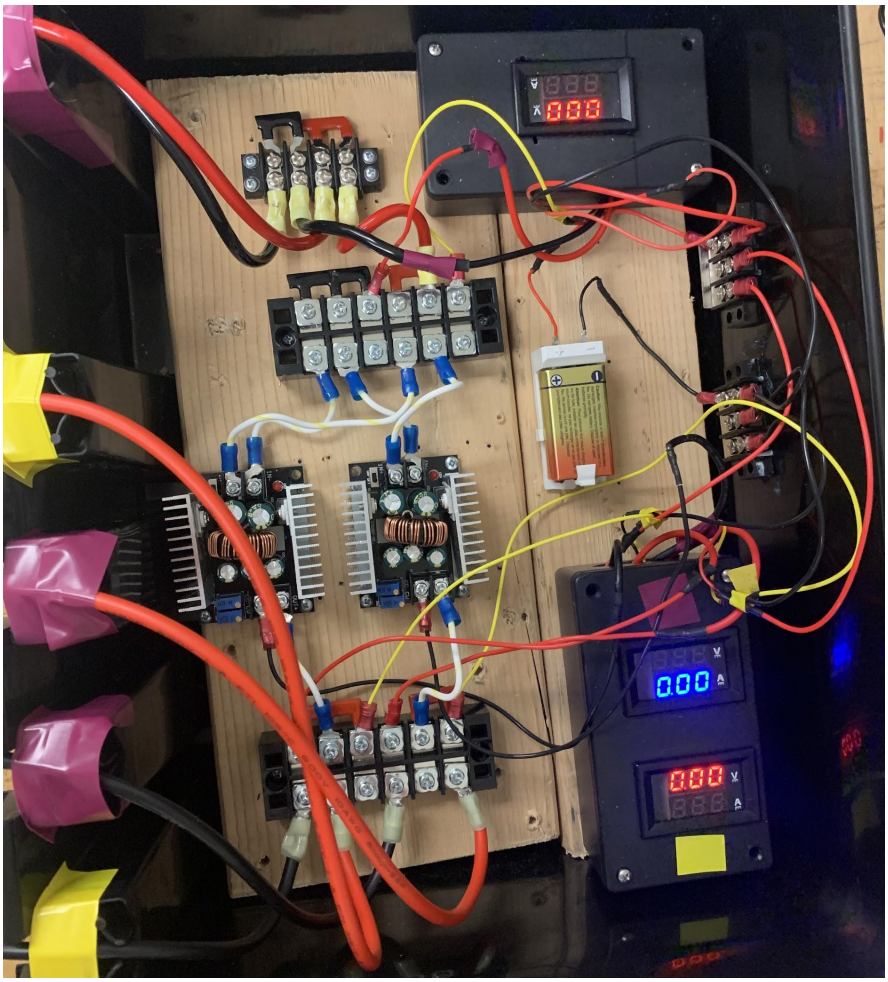

Fig. 5 Overall circuit design

To power these volt/ammeters, they require an external voltage source of 5–40 V DC. Used in this circuit is a 9-V alkaline battery (Fig. 6). This one battery is used to power all three volt/ammeters using a screw terminal and pre-insulated terminal barrier strips.

Fig. 6 Battery for powering volt/ammeter display

2.4 Electrolysis Cell

The electrolysis cell contains the potassium hydroxide (KOH) solution and two electrodes, which, when supplied with a sufficient voltage and current, produce hydrogen and oxygen gas. H-cells allow for each electrode to have its own housing, but still allow charge transport through the opening between separate compartments. Most in lab H-cells were made up of glass, which is fragile. To prevent breaking, the H-cell was constructed out of 0.25-inch acrylic plexiglass sheets. This cell was designed in SolidWorks, consisting of five unique parts: top, bottom, back, front and side (two copies) (Fig. 7). Each part was then laser cut using the Epilog laser cutter. Once two individual cubes are made, they were glued together in order to create the H-cell.

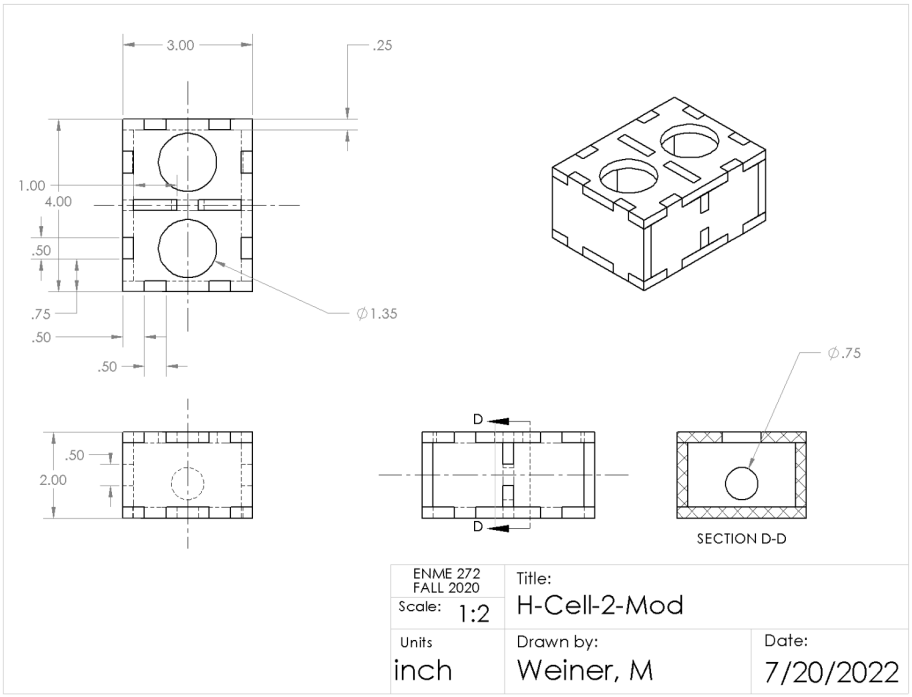

Fig. 7 H-cell assembly technical drawing

The design allows for insertion of a rubber stopper on the top of the cell. The stopper is machined to allow for the insertion of the electrode, while still protecting the cell from the external environment. Shown in Fig. 8 is the constructed cell with an example tubing shown. When in use, there would be a separate tube and copper wire in each stopper. To secure the parts together and prevent leaking through cracks, a silicone adhesive was used.

Fig. 8 Assembled H-cell with feedthrough connectors

The copper wire has the electrode connected to one end submerged in the KOH, while the other end is exposed outside, which allows for the connection into the circuit. The electrode is attached to the wire using a solution of silver (Ag) and acetone to ensure a conductive joining contact. Once the acetone has evaporated, epoxy is placed on top and let to set for 24 h. For this system, the specific electrodes used are 0.3-mM iron (Fe)-doped cobalt phosphide (Co_2P) on nickel foam as the anode and Co_2P on nickel foam for the cathode (Fig. 9).

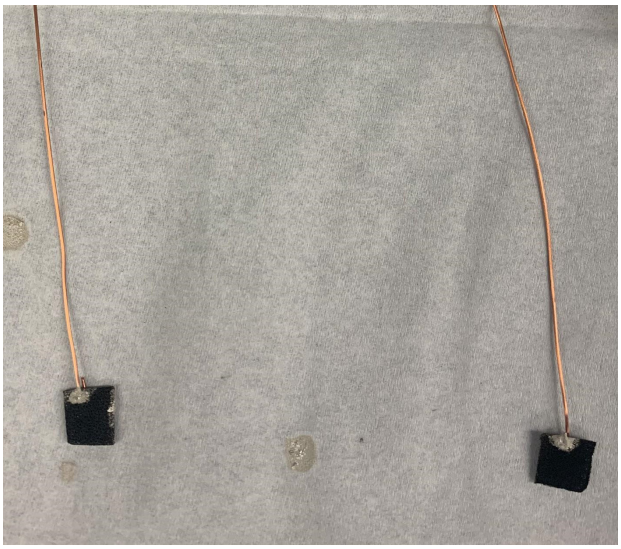

Fig. 9 Assembled electrodes

The tubes are connected to multi-layer foil gas sampling bags[9] (Fig. 10) to collect oxygen and hydrogen gas, which enables an accurate measurement of the volume of hydrogen gas created and subsequent energy generated. The tubing connected to the gas bag is glued into the stopper within the H-cell. This is to ensure optimal collection of hydrogen, as well as to seal possible gas leaks. These aluminum bags can contain up to 1 L of hydrogen gas.

Fig. 10 Avantor multi-layer foil gas sampling bag

2.5 Physical Design

The physical design of the system needs to be environmentally resilient: accounting for weather, temperature, animals, and any other environmental factors. The main components of the physical design include the structural housing and electronics box.

The structural housing needs to hold the solar cell in place, be tall enough to allow the electronics box to fit underneath, and sturdy enough to not fall over due to wind or small animals. To meet these requirements, the housing was constructed from 30- × 30-mm T-slotted anodized aluminum rails (Fig. 11). The rails were then cut to the correct size and assembled together using 30-mm T-slotted corner brackets. This design allows for the solar cell to be easily removed and inserted into the housing.

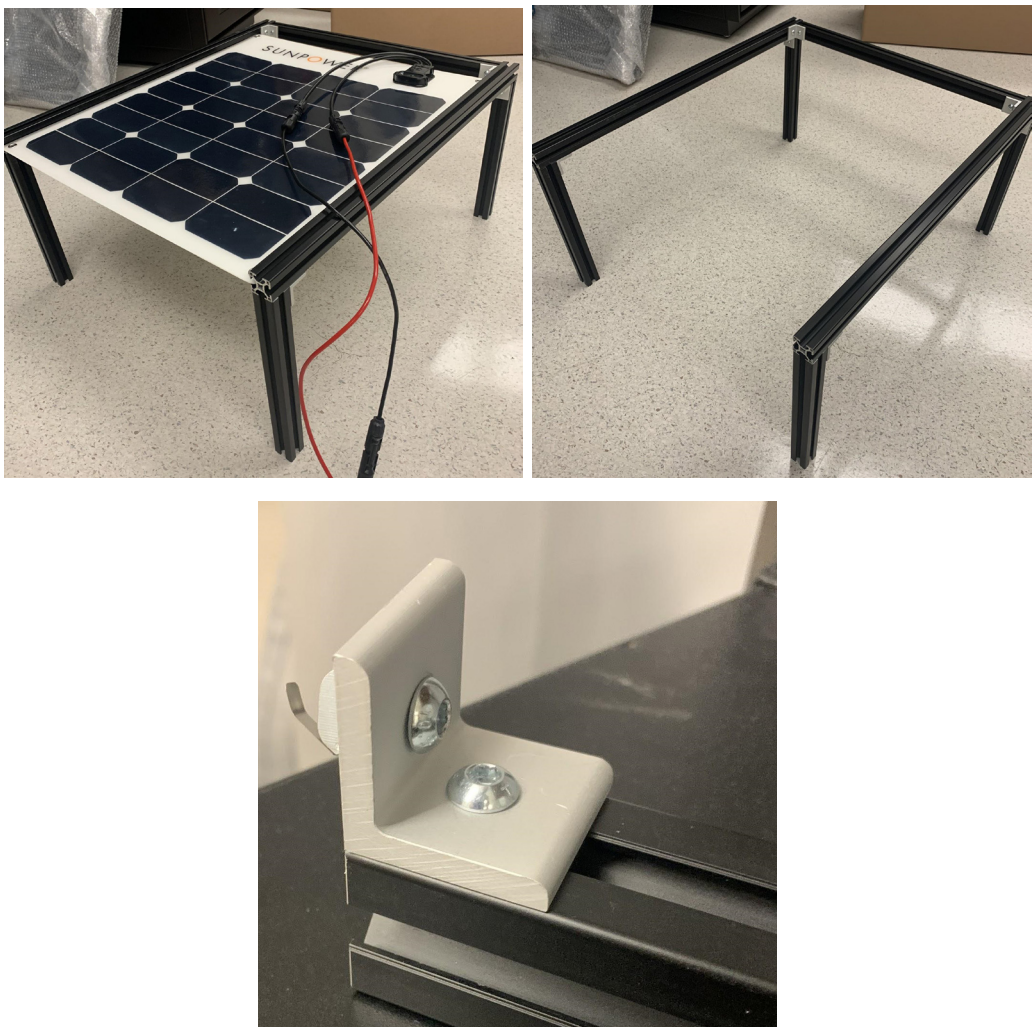

Fig. 11 Assembled aluminum T-slotted rail and corner bracket structure to house solar panel

The electronics box used is the SockitBox weatherproof connection box (Fig. 12). The box is marketed as being water-, snow-, and dirt-proof. Due to previous testing of the buck converters, temperature inside the box is not a large concern; therefore, there is no need to engineer the box for ventilation and exposing the interior of the box to the outside environment. The box also comes with silicone molds, which are able to compress and seal the wires going in and out of the box.

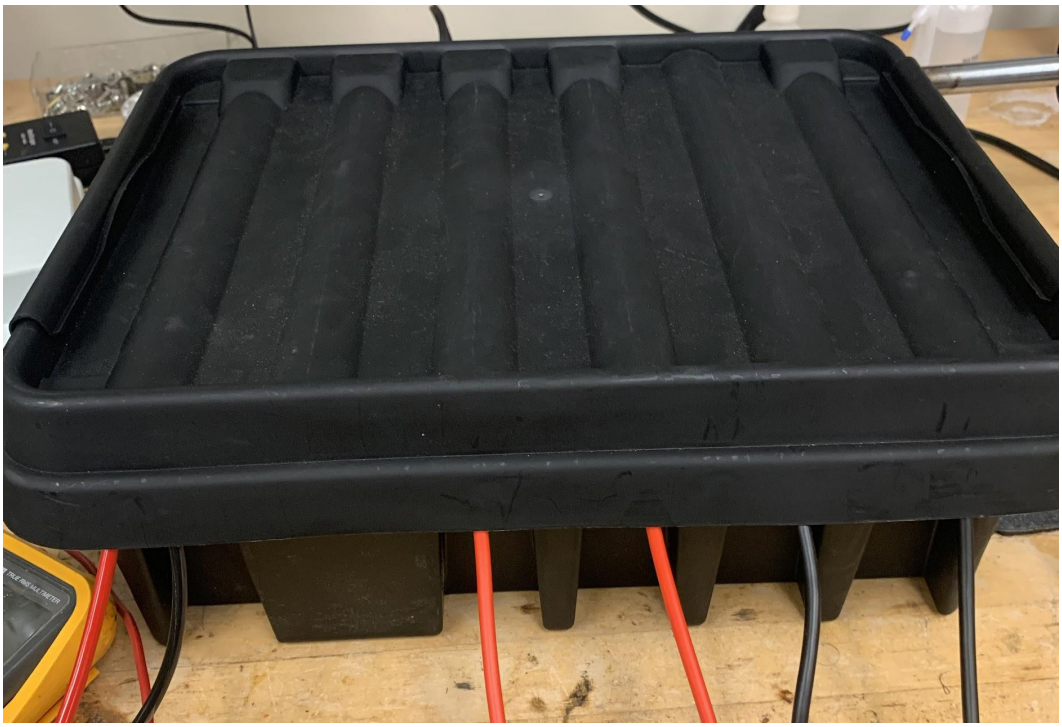

Fig. 12 Weatherized electronics box

2.6 Estimated Weight of System Bill of Materials (BOM)

As shown in Table 1, the bulk of the weight in the system comes from parts, which can be greatly reduced. The PV cell used for the system had a much greater power capacity than what was used for the electrolyzer. If the PV module is smaller, then the amount of rails needed also decreases. Also, a much smaller weatherized box could be utilized based on the size of the electrolyzer, which would decrease the amount of wood used for mounting.

Table 1 BOM

System component	Item name	Weight per unit	Unit	Amount used	Mass (g)	Mass (kg)	Total system mass (kg)
PV system					**3906.485**	3.906485	8.020909
	PV cell	1100	g/unit	1	1100		
	T-slotted aluminum rails	20.67	g/in	125.5	2594.085		
	Corner bracket	35.4	g/unit	6	212.4		
Electronics box					**3598.33**	3.59833	
	Weatherized box	821	g/unit	1	821		
	9-V alkaline battery	45	g/unit	1	45		
	Battery holder	10.3	g/unit	1	10.3		
	Buck converters	90.71	g/unit	2	181.42		
	Single series connector	0.825	g/unit	14	11.55		
	Fork terminal	2.64	g/unit	36	95.04		
	10-AWG wire	1.56	g/in	504	786.24		
	18-AWG wire	0.31	g/in	84	26.04		
	Screw terminal	11.33	g/unit	8	90.64		
	Volt/ammeter	80	g/unit	3	240		
	MC4 connector	21.4	g/unit	11	235.4		
	Wood plank	6.9	g/in^2	153	1055.7		
Electrolyzer					**516.094**	0.516094	
	KOH volume added	1.05	g/ml	150	157.5		
	Hydrogen evolution reaction (HER) stopper	56.6	g/unit	1	56.6		
	Oxygen evolution reaction (OER) stopper	57.8	g/unit	1	57.8		
	Catalyst (2–720 mm^2)	0.0008986111111	g/mm^2	1440	1.294		
	H-cell	205.6	g/unit	1	205.6		
	Hydrogen bag	14.5	g/unit	1	14.5		
	Tray	22.8	g/unit	1	22.8		

3. Testing and Validation

While constructing the circuit, various instruments were used to ensure it was working correctly.

3.1 Circuitry Validation

A multimeter and voltage source were used to validate that all connections made in the circuit were conductive. The multimeter was first used across all connections to perform continuity tests. Once all connections were validated, a voltage source was used in place of the solar cell to input a steady voltage into the circuit. Using a

multimeter, various readings were tested to make sure that the circuit was outputting the correct voltage and current. Lastly, a multimeter was used while tuning the buck converters to ensure that output voltage to the electrolyzer was controllable.

3.2 Electrolysis Testing

To test the electrolytic catalyst's effectiveness, three different types of tests were run: cyclic voltammetry (CV), linear sweep voltammetry (LSV), and electrochemical impedance spectroscopy (EIS). All electrolysis tests were carried out on a Gamry Reference 3000 potentiostat. The setup used for this experiment consisted of three electrodes. The reference electrode used was silver-silver chloride (Ag/AgCl), the working electrode was the catalyst, and the counter electrode was a platinum spiral wire. The electrolyte is 1-M KOH. The current density was calculated using the 1-D surface area of the catalyst. All measured potentials were converted to the reversible hydrogen electrode (RHE) via the Nerst equation: $E_{RHE} = E_{Ag/AgCl} + 0.059\ pH + 0.197$, where E_{RHE} is the potential against RHE and $E_{Ag/AgCl}$ is the measured potential against the reference electrode Ag/AgCl.

3.2.1 Oxygen Evolution Reaction Testing (CV)

CV was used to test the effectiveness of the OER catalyst. The catalyst was pre-stabilized by running a CV at a scanning rate of 20 mV/s for 50 cycles within the potential window of 0 to 0.8 V versus Ag/AgCl. The OER performance was then quantified via a CV test with a scanning rate of 1 mV/s

Figure 13 displays the results of the tests, which show that the addition of Fe doping to the catalyst reduced the voltage in which a current density of 10 mA/cm^2 was reached (this voltage is designated as η_{10}). A small overpotential η_{10} of 240 ± 4 mV was achieved with the presence of Fe doping, while the non-doped catalyst has an η_{10} of 280 ± 4 mV. Based on this, oxygen production efficiency can be increased by introducing Fe doping to Co_2P on nickel foam for the anode.

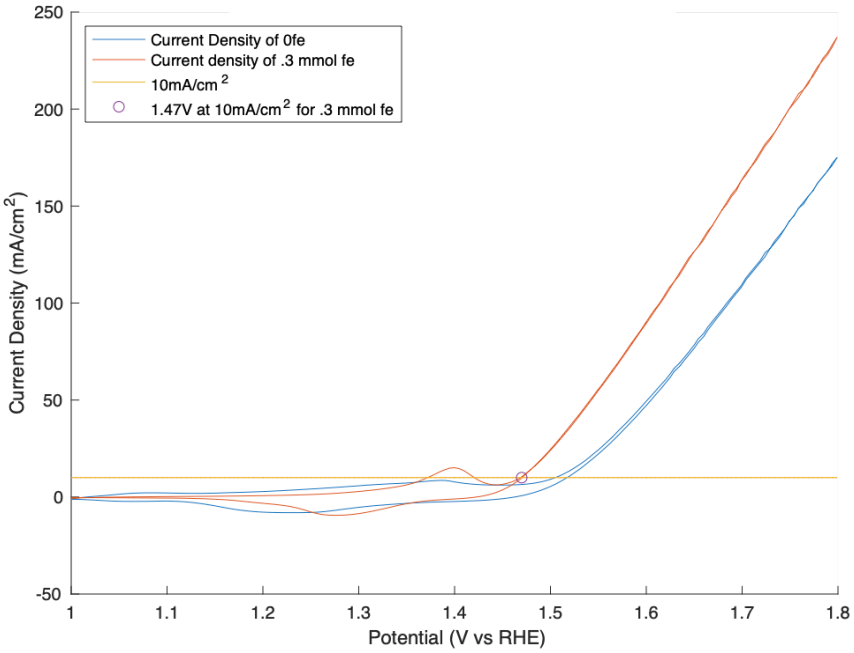

Fig. 13 CV: current density vs. potential (V vs. RHE) for OER reaction of Co_2P on nickel foam

3.2.2 Hydrogen Evolution Reaction Testing (LSV)

LSV was used to choose the most effective catalyst for HER. The setup used was the same as the CV test for OER. Again, current density is used to demonstrate the catalysts' ability to produce hydrogen. As shown in Fig. 14, the addition of Fe doping has an adverse effect on the current density of the catalyst, necessitating the usage of Co_2P on nickel foam as the catalyst for the HER. At an applied potential of –0.2 V versus RHE, the non-Fe-doped catalyst achieved a current density of 39 mA cm^{-2}, while the Fe-doped catalyst achieved only 24 mA cm^{-2}. An overpotential of η_{10} of 160 ± 4 mV was achieved with the presence of Fe doping, while the non-doped catalyst has an η_{10} of 120 ± 4 mV.

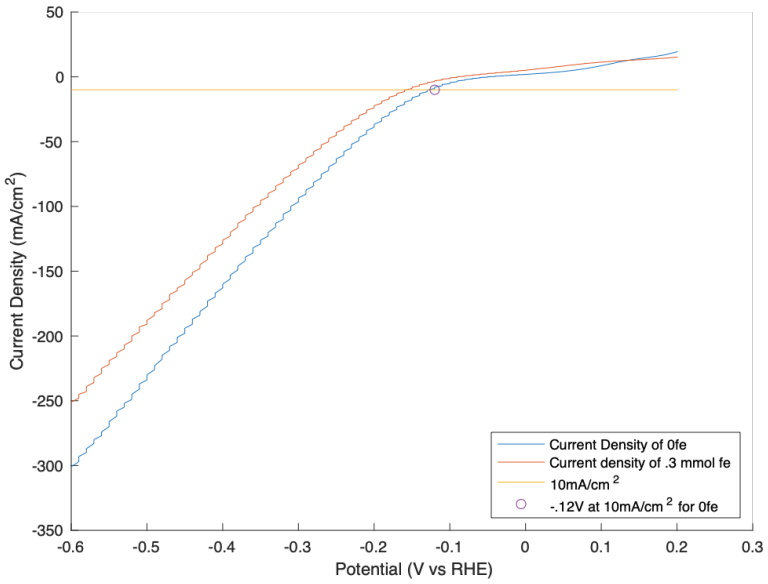

Fig. 14 LSV: current density vs. potential (V vs. RHE) for HER reaction of Co_2P on nickel foam

3.2.3 Overall Reaction (EIS and LSV)

To evaluate the overall water splitting reaction, both an EIS and LSV test were conducted. Both these tests used the same two-electrode setup. The working electrode was the catalyst chosen for HER and the counter electrode was the catalyst chosen for OER. Using the Gamry software, an EIS test was run at both 2.0 and 1.7 V (versus the reference) from 100 kHz to 0.1 Hz. For the electrolysis reaction, the resistance at high frequencies is important. The resistance at high frequencies was found to fluctuate between 17 and 18 Ω at 1.7 V. Shown in Fig. 15 is the EIS spectra for overpotentials of 470 and 670 mV. Resistance is important because $I = \frac{V}{R}$. Therefore, the smaller the resistance at high frequencies, the greater the current will be during the electrolysis reaction leading to a greater hydrogen production rate. This illustrates an important finding: The greater the voltage, the more efficient the reaction will be.

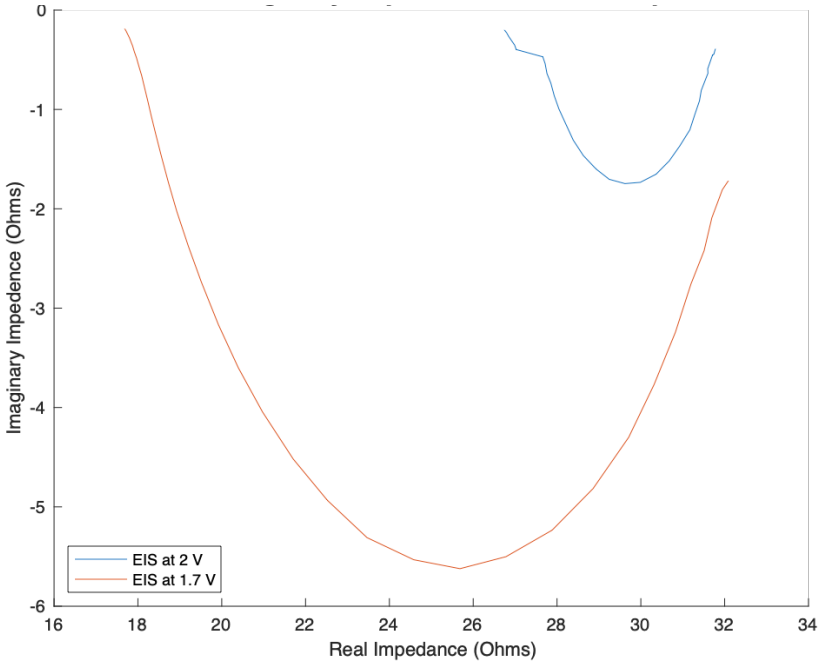

Fig. 15 EIS curve of imaginary impedance vs. real impedance for using Fe-doped Co_2P and Co_2P on nickel foam for OER and HER

The LSV test ran from 0 to 2.25 V at a scanning rate of 50 mV/s (Fig. 16). The test shows that a current density of 10 mA/cm^2 was achieved at roughly 1.55 V, which is lower than the expected 1.59 V based on the individual OER and HER tests.

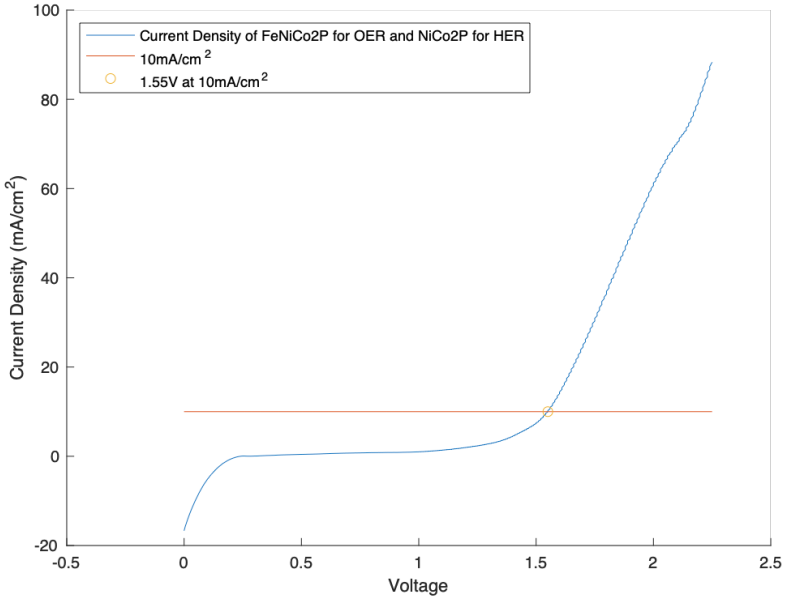

Fig. 16 LSV: current density vs. voltage for overall reaction of Co_2P and Fe-doped Co_2P on nickel foam as the cathode and anode, respectively

3.2.4 Long-Term Stability Testing

To test the long-term stability of the electrolysis reaction, a multiple-step chronoamperometry test was run (Fig. 17). Using the same set up as the EIS and LSV of the overall reaction, the voltage was held constant at 2 V (versus reference) for 8 h, then at 3 V for 8 h, and 2 V for the final 8 h. The current was sampled every 3 s. As shown in Fig. 17, the catalyst exhibits strong stability at 2 V, with slightly more noise at 3 V. This shows a key tradeoff that while the reaction is more efficient at higher voltages, it is also more unstable.

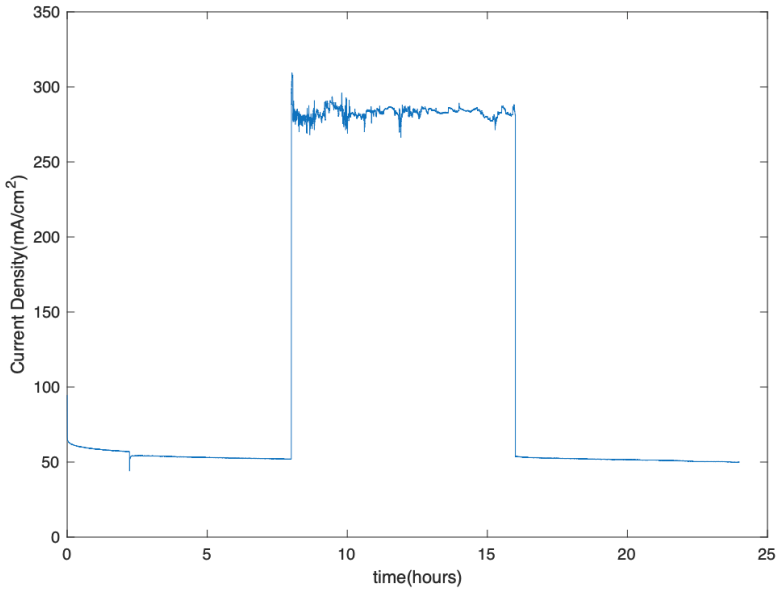

Fig. 17 Chronoamperometry-based long-term stability test of Co_2P and Fe-doped Co_2P on nickel foam as the cathode and anode, respectively. Held at 2 V in the first portion, 3 V in the second, and 2 V.

3.3 Environmental Tests

Environmental conditions will determine the system performance of the PV cell. These conditions include shadowing and particulate matter to simulate dust. These factors are to be examined to demonstrate their influence on hydrogen production. A baseline procedure will investigate the voltage and current outputs produced from the PV cell in typical conditions (clear and cloudy skies); these measurements will be the control for this experiment. Data from these tests provide findings that will be used to make adjustments tuning the buck converters for optimal hydrogen output.

3.3.1 PV Output Affected by Shadows

Varying obstruction factors (shadowing and debris) are individually tested on the PV-electrolyzer to observe any notable changes to the system's outputs and gather a data-driven model of its behavior beyond the typical conditions that were tested as a baseline. Panels made from thick cardstock are used to block different rows and columns of the PV including the top, bottom, left, right, as well as 50% and 75% of the panel. The voltage and current outputs are recorded for both the PV (read from the first volt/ammeter in the electronics box) and appropriate buck converter connected to the load. In initial testing, this load was modeled using a 14.7-Ω resistor rated for 5 W, which was later replaced with the electrolysis cell. Figure 18 shows the shadowing effect on power output.

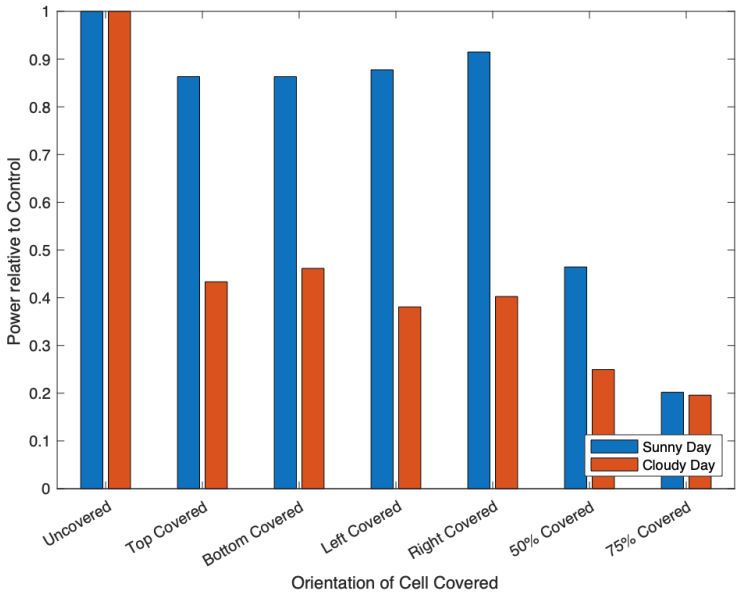

Fig. 18 Shadowing effect on power output, relative to control, of solar panel on sunny and cloudy day

3.3.2 PV Output Affected by Debris

To simulate debris, flour is used as it best represents fine contaminants that are more likely to contribute to soiling on a PV in a field setting, such as soot, wind-blown dust, and pollen. The debris was incrementally dusted in dust deposition densities ranging from 1 to 300 g/m^3 onto the PV module and observed for any impacts to the solar-powered water splitting engaging in the electrolysis cell (Fig. 19). Interestingly, none of the trials impacted system performance enough to terminate the electrolysis taking place or hydrogen production.

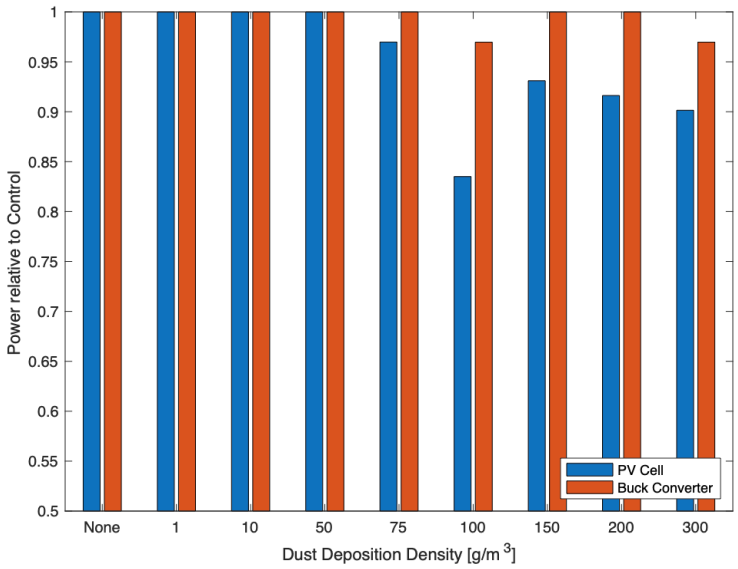

Fig. 19 Dust deposition density effect on power output, relative to control, of solar panel and buck converters

3.4 In-Lab Hydrogen Testing

Using the 30-mm^2 1-D surface area catalyst, hydrogen production was measured while indoors. A potential of 3 V was applied across the electrodes for 16 h. The same setup described in Section 2.4 was used. To quantify the volume of hydrogen collected throughout the experiment, a water displacement method was used. The total volume of hydrogen was found to be 0.1861 L. Using the environmental temperature of 20 °C gives 24.026-L/mol H_2. By integrating current versus time, Q is found to be 3.373E3 C. This results in a Faradaic efficiency of 44.31%. Integrating electrical power versus time going through the electrolyzer gives a total input energy of 10.12 kJ. Using 120 MJ/kg as the energy density of hydrogen gas and 2.016-kg/mol H_2, the calculated chemical stored energy is 1.874 kJ, giving an input to output energy efficiency of 18.52%. Also, the Faradaic efficiency was found to be 44.31%. Over the entirety of the experiment, the average resistance within the cell while running the reaction was 51.2265 Ω.

Using the 320-mm^2 1-D surface area catalyst, hydrogen production was also measured while indoors. A potential of 5 V was applied across the 320-mm^2 electrodes for almost 5 h. Hydrogen testing from the 320-mm^2 catalyst follows the same outlined procedures as the 30-mm^2 catalyst. The 320-mm^2 catalyst produced 0.637 L of hydrogen, a total input energy of 25.706 kJ, and a calculated chemical stored energy of 6.4137 kJ, giving an input to output energy efficiency of 24.95%. The resulting Faradaic efficiency of the 320-mm^2 catalyst is 99.51%.

3.5 Outside Hydrogen Testing

Using the 320-mm^2 1-D surface area catalyst, hydrogen production was measured while outdoors. The entire system setup discussed in Section 2 was used. The buck converters were set to allow a maximum of 5 V into the electrolyzer, and the current and voltage readings were monitored once an hour. Due to the current being greater than 40 mA, no continuous data logging tools were utilized. The electrolyzer ran for about 2 h and 50 min, producing a measured 0.4366 L of H_2 gas. Based on the four discrete data points, which were recorded throughout runtime, the total electrical energy and total charge delivered into the cell were found to be 25.06 kJ and 5.02×10^3 C. Using 120 MJ/kg as the energy density of hydrogen gas and 2.016-kg/mol H_2, the calculated chemical stored energy is 4.251 kJ giving an input to output energy efficiency of 16.96%. Also, the Faradaic efficiency was found to be 67.53%.

Using the 720-mm^2 1-D surface area catalyst, hydrogen production was measured while outdoors. The entire system setup discussed in Section 2 was used. The buck converters were set to allow a maximum of 6.5 V into the electrolyzer, and the current and voltage readings were monitored once an hour. The electrolyzer ran for about 1 h and 30 min, producing a measured 0.515 L of H_2 gas. Based on the three discrete data points, which were recorded throughout runtime, the total electrical energy and total charge into the cell were found to be 51.76 kJ and 7.97×10^3 Columbs. Using 120 MJ/kg as the energy density of hydrogen gas and 2.016-kg/mol H_2, the calculated chemical stored energy is 5.01 kJ giving an input to output energy efficiency of 9.69%. Also, the Faradaic efficiency was found to be 50.24%.

3.6 Hydrogen Collection Discussion

After evaluating the results, the electrical to chemical efficiencies clearly followed their theoretical pattern of 1.23/V, where V is the applied voltage. This relationship shows that the system is most efficient with respect to energy, at the lowest possible voltage needed to carry this reaction. However, with respect to time, the system is most efficient at higher voltages. Given that the resistance seems to decrease as the voltage increases, current is exponentially correlated with an increase in voltage. This is a tradeoff that needs to be optimized in future work. When testing outside, the temperature was approximately 30 ℃, compared to the 20 ℃ in the lab. Based on the results, there is a clear correlation between temperature and speed of the reaction, because there was a smaller resistance at higher temperatures.

One main issue which was encountered through the course of these experiments was that hydrogen collection did not match its theoretical value. This can be due to

many reasons; however, based on observations of where the bubbles go throughout the experiment, the most obvious source of error is due to the volume in which the hydrogen gas needs to fill before rising into the bag. This volume should be mitigated in order to observe the best results.

4. Conclusion

In summary, this work is a demonstrator basis for constructing a system connecting a PV module to a water electrolysis cell for outdoor operation. The system successfully converts incident solar energy into hydrogen gas, and the metrics of Faradaic efficiency and energy are quantified. Several practical aspects of the design are addressed, including voltage and current regulation, construction materials for the H-cell, electrocatalyst synthesis, and testing methodologies. Future system design work will include using the additional solar energy from the PV module to charge an on-board lithium ion battery pack to enable more versatile usage for electrical-demand applications, additional weatherproofing to allow for usage in a variety of environments, and better physical integration of components for more ease of portability.

Additionally, this demonstrator is a method for fundamental research in energy conversion technologies, including: plasmonic light-to-heat transfer, solar light absorption, and electrocatalysis for producing higher-order hydrocarbons. If these laboratory-level research technologies are transferred into the demonstrator system, it then gives a first-step practical implementation for these technologies outside of the laboratory and with quantifiable metrics.

5. References

1. Department of the Army. The U.S. Army in Multi-Domain Operations 2028. TRADOC Pamphlet 525-3-1. Army (US); 2018.
2. United States Army climate strategy. Department of the Army, Office of the Assistant Secretary for Installations, Energy, and Environment; 2022.
3. Trautz KM, Jenkins PP, Walters RJ, Scheiman D, Hoheisel R, Tatvarti R, Chan R, Miyamoto H, Adams JGJ, Elarde VC, et al. Mobile solar power. IEEE Journal of Photovoltaics. 2013;3(1).
4. Ames B. Nanotechnology delivers military power. Military & Aerospace Electronics. 2005.
5. SPR-E-flex-50. SunPower; n.d. [accessed 2022 July 11]. https://us.sunpower.com/sites/default/files/50w-flexible-panel-spec-sheet-0_0.pdf.
6. Male/female solar panel cable connectors. Renogy; n.d. [accessed 2022 July 11]. https://uk.renogy.com/renogy-mc4-malefemale-solar-panel-cable-connectors-5-pair/.
7. Step down buck converter/regulator. Electronics Notes; n.d. [accessed 2022 July 25]. https://www.electronics-notes.com/articles/analogue_circuits/power-supply-electronics/switching-step-down-buck-regulator-dc-dc-converter.php#:~:text=The%20fundamental%20circuit%20for%20a,receives%20energy%20from%20the%20source.
8. 0.28 inch mini digital voltmeter ammeter DC 100V 10A panel amp volt current meter tester 0.28 inch dual LED display. DIY More; n.d. [accessed 2022 July 25]. https://www.diymore.cc/products/0–28-inch-mini-digital-voltmeter-ammeter-dc-100v-10a-panel-amp-volt-current-meter-tester-0–28-inch-dual-led-display.
9. Multi-layer foil gas sampling bags, Restek. Avantor VWR; n.d. [accessed 2022 July 25]. https://us.vwr.com/store/product/18812758/multi-layer-foil-gas-sampling-bags-restek.

Appendix. Parts List Purchase Links

- Buck converters:
    - https://www.amazon.com/Aceirmc-Converter-Adjustable-Regulator-Protection/dp/B0823MM1DV
- Voltmeter/ammeter displays:
    - https://www.diymore.cc/products/0–28-inch-mini-digital-voltmeter-ammeter-dc-100v-10a-panel-amp-volt-current-meter-tester-0–28-inch-dual-led-display
- Gas sampling bag:
    - https://us.vwr.com/store/product/18812758/multi-layer-foil-gas-sampling-bags-restek
- Weatherproof electronics box:
    - https://www.amazon.com/gp/product/B018HHMBW2
- Solar cell:
    - https://us.sunpower.com/sites/default/files/50w-flexible-panel-spec-sheet-0_0.pdf

List of Symbols, Abbreviations, and Acronyms

1-D	one-dimensional
Ag	silver
Ag/AgCl	silver-silver chloride
ARL	Army Research Laboratory
AWG	American wire gage
BOM	bill of materials
Co_2P	cobalt phosphide
CV	cyclic voltammetry
DC	direct current
EIS	electrochemical impedance spectroscopy
Fe	iron
HER	hydrogen evolution reaction
KOH	potassium hydroxide
LSV	linear sweep voltammetry
MDO	Multi-Domain Operations
OER	oxygen evolution reaction
PV	photovoltaic
PWM	pulse width modulation
RHE	reversible hydrogen electrode

1 (PDF)	DEFENSE TECHNICAL INFORMATION CTR DTIC OCA
1 (PDF)	DEVCOM ARL FCDD RLD DCI TECH LIB
3 (PDF)	DEVCOM ARL FCDD RLS CC V PARAMESHWARAN D BAKER J LI
2 (PDF)	UMD COLLEGE PARK M WEINER B KHAN
1 (PDF)	UMBC L GARCIA